https://doi.org/10.5194/egusphere-2024-3380
Preprint. Discussion started: 13 November 2024

Application of quality-controlled sea level height observation at the central East China Sea: Assessment of sea level rise

Taek-bum Jeong[1,2], Yong Sun Kim[3,7], Hyeonsoo Cha[4], Kwang-Young Jeong[5], Mi-Jin Jang[3], Jin-Yong Jeong[6], and Jae-Ho Lee[3*]

[1]Center for Climate Physics, Institute for Basic Science, Busan, Republic of Korea, 46241

[2]Pusan National University, Busan, Republic of Korea, 46241

[3]Ocean Circulation Research Center, Korea Institute of Ocean Science and Technology, Busan, Republic of Korea, 49111

[4]Center for Sea-Level Changes, Jeju National University, Jeju, Republic of Korea, 63243

[5]Ocean Research Division, Korea Hydrographic and Oceanographic Agency, Busan, Republic of Korea, 49111

[6]Marine Disaster Research Center, Korea Institute of Ocean Science and Technology, Busan, Republic of Korea, 49111

[7]Ocean Science, University of Science and Technology, Daejeon, Republic of Korea, 34113

Correspondence to: Jae-Ho Lee (Jaeholee@kiost.ac.kr)

Abstract. This study presents the state-of-the-art quality control (QC) process for sea level height (SLH) time series observed at the Ieodo Ocean Research Station (I-ROS) in the central East China Sea, a unique in-situ measurement in the open sea for over two decades with a 10-minute interval. The newly developed QC procedure called the Temporally And Locally Optimized Detection (TALOD) method has two notable differences in characteristics from the typical ones: 1) spatiotemporally optimized local range check based on the high-resolution tidal prediction model TPXO9, 2) considering the occurrence rate of a stuck value over a specific period. Besides, the TALOD adopts an extreme event flag (EEF) system to provide SLH characteristics during extreme weather. A comparison with the typical QC process, satellite altimetry, and reanalysis products demonstrates that the TALOD method can provide reliable SLH time series with few misclassifications. Through budget analysis, it was determined that the sea level rise at I-ORS is primarily caused by the barystatic effect, and the trend differences between observations, satellite, and physical processes are related to vertical land motion. It was confirmed through GNSS that ground subsidence of –0.89±0.47 mm/yr is occurring at I-ORS. As a representative of the East China Sea, this qualified SLH time series makes dynamics research possible spanning from a few hours of nonlinear waves to a decadal trend, along with simultaneously observed environmental variables from

https://doi.org/10.5194/egusphere-2024-3380
Preprint. Discussion started: 13 November 2024

the air-sea monitoring system in the research station. This TALOD QC method is designed for SLH observations in the open ocean, but it can be generally applied to SLH data from tidal gauge stations in the coastal region.

1 Introduction

Sea Level Height (SLH) comprises oceanic components such as tides and currents and atmospheric components (Pirooznia et al., 2016). Global warming due to the increased greenhouse gas has caused a persistent increase of heat fluxes into the ocean, accelerating upper ocean heat content and the loss of land-based glaciers and ice sheets, resulting in rapid sea level rise (SLR; Pugh, 2019; IPCC). This rise is not spatially homogeneous but localized in association with a change in the current system (*e.g.,* Roemmich et al., 2007; Hamlington et al., 2020; Lee et al., 2022; Li et al., 2024). Rising sea levels have induced coastal erosion and broad flooding, suggesting a presumable vulnerability of populated low-lying coastal regions to global warming (Kulp and Strauss, 2019). Recent research has demonstrated its robust relationship with extreme weather events (Cayan et al., 2008; Yin et al., 2020; Calafat et al., 2022), underscoring the need for a long-term SLH monitoring network.

A global network of tidal gauges at the coastal region, along with satellite altimetry for the open ocean, has made it possible to observe worldwide sea level changes (*e.g.,* Dieng et al., 2017; Cazenave et al., 2018; Chen et al., 2017; Royston et al., 2020; Cha et al., 2023). The upward trend of global mean SLR increased from 3.05 mm/yr for the period 1993–2018 to 3.59 mm/yr from 2006 to 2018, about twice faster than 1.7 mm/yr during the 20th century (Fox-Kemper et al., 2021; Nerem et al., 2018). A future projected sea level trend is expected to be 4.63±1.1 mm/yr for the period 2010–2060 from observed and reconstructed measurements around Korea (Kim and Kim, 2017), implying more frequent occurrences of extreme weather and climate hazards associated with the mean sea level rising within the near future.

Due to its broad socioeconomic implications, the Korea Hydrographic and Oceanographic Agency (KHOA) has constructed a sea level monitoring network with thirty-eight tide gauge stations for the coastal region around Korea (red pentagram in Fig 1). Besides, the ocean research stations, steel framed tower-type research facilities, started to conduct unceasing and autonomous observations to cover a north-south section of the Yellow and East China Seas, allowing us to understand air-sea interaction and atmospheric and oceanic processes in various time scales at the open ocean (Ha et al., 2019; Kim et al., 2019; Kim et al., 2022; Kim et al., 2023a; Kim et al 2023b; Saranya et al., 2024). The Ieodo ocean research station (I-ORS), the first one constructed at 32.125°N, 125.18°E (see Fig. 1 for its location) in 2003, has produced sea level measurements using a radar-type sensor with a 10-minute interval for more than two decades since October 2003. This station is strategically positioned along the

https://doi.org/10.5194/egusphere-2024-3380
Preprint. Discussion started: 13 November 2024

pathway of typhoons that impact the Korean Peninsula; hence, the I-ORS can serve as a crucial platform for comprehending extreme weather phenomena (Moon et al., 2010; Park et al., 2019; Yang et al., 2022) and long-term climate variability.

The collected sea level data, however, contains intricate outliers such as missing, spike, electric noise, stuck, drift, systematic conversion (or offset)[1], and so on (Pytharouli et al., 2018). These outliers must be identified or corrected before being used for research. This process, known as Quality Control (QC), involves outlier classification into range, variability (or gradient), and sensor test categories (OOI, 2013; Min et al., 2020). Each institution utilizes a different algorithm. For instance, outliers might be identified by applying a threshold of three times the standard deviation above and below the average of measurements within a specified sliding window (Min et al., 2020; 2021). This approach assumes the Gaussian distribution of the observed time series; hence, it may not be suitable for uniformly applying this method because nonlinear waves or abrupt extreme events tend to be misclassified as outliers. Also, the variables that are greatly affected by strong tides may have difficulty detecting outliers when a range check is performed without considering tidal components. Therefore, Pugh (1987) suggested a QC procedure based on tidal components estimated by a harmonic analysis. Recently, Pirooznia et al. (2019) computed tides by adopting the classical least square (CLS) and total least square (TLS) from raw data that contained outliers and missing values. They used the estimated tidal components to get residual components of SLH data and then performed outlier detection. This process might be appropriate for the data stably obtained from tide gauge stations but seems impertinent to measurements in the open ocean, which may have various types of intricate outliers.

In addition, previous studies attempted to verify the factors contributing to sea level rise (SLR) using various data. Cha et al. (2023) quantified and assessed the underlying processes contributing to sea level rise in the northwestern Pacific using reanalysis data and satellite measurements from 1993 to 2017. This study found that the major contributions to sea level rise are land ice melt and sterodynamic components, while the spatial pattern and interannual variability are dominated by the sterodynamic effect. However, satellite-based sea level observations cannot detect vertical land motion such as subsidence or uplift, which may lead to trend differences between

[1] The I-ORS methodology for sea level measurements was changed in December 2007. Previously, the I-ORS observed the length between the instrument and the sea level; since then, it has been changed to observe the sea level to the bottom. Due to the methodological switch, the recorded sea level time series has a sharp and systematic offset, as described in section 2.1.

https://doi.org/10.5194/egusphere-2024-3380
Preprint. Discussion started: 13 November 2024

satellite and station observation. This indicates the need to analyze the variability of vertical land motion at these stations as well.

This paper aims to introduce a unique, invaluable SLH time series obtained in the open ocean over two decades, processed with a newly developed QC process named the Temporally And Locally Optimized Detection (TALOD) method. For this purpose, we take advantage of simulated tidal components based on TOPEX/Poseidon global tidal model v9 (TPXO9; Erofeeva and Egbert, 2018). This high-resolution global tidal model reproduces tidal well components around the Korean peninsula (Lee et al., 2022) and, hence, can be used for a local and temporal range check. The performance of the newly suggested QC process is assessed by comparing it to a typical QC method suggested by the Intergovernmental Oceanographic Commission (IOC), and the qualified, daily and monthly averaged sea level time series are assessed using satellite altimetry and reanalyzed products from GLORYS12, ORAS5, and HYCOM regarding their long-term trends. Additionally, the physical processes contributing to sea level rise at the I-ORS were analyzed using reanalyzed product, and the vertical land motion at the I-ORS platform was estimated using the Global Navigation Satellite System (GNSS).

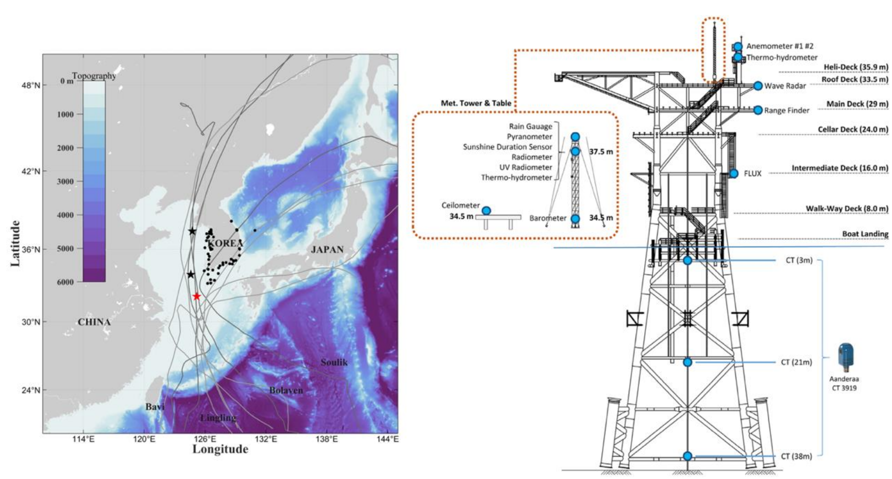

Figure 1. The structure of I-ORS and Instruments (Right) and the horizontal distribution for bathymetry and the tracks of typhoon passed by I-ORS (data from Joint Typhoon Warning Center; cases depicted in Fig. 10). The star marks indicate the location of the I-ROS (red) and the Socheongcho (black; above) and Gageocho (black; below) Ocean Research Station, respectively. The black dots depict the locations of tide stations. The grey solid lines show the storm tracks passing by I-ROS from 2003 to 2022. The darker lines indicate the typhoon case in Table 2.

https://doi.org/10.5194/egusphere-2024-3380
Preprint. Discussion started: 13 November 2024

2 Data and Method

2.1 SLH observed time series from the I-ORS

We constructed the TALOD QC process based on the TPXO9 and applied it to the 10-minute interval real-time SLH measurements obtained from the I-ORS, a total of 1,011,584 data points from 8 October 2003 to 31 December 2022. The data was measured by the MIROS SM-140 non-directional wave radar, installed at the main deck 29 m above the sea surface (Fig. 1). The range finder principally estimates the distance to the sea surface through the reflected signals by detecting back-scattered microwaves from the surface. Table 1 describes the detailed specification of the SM-140. The sensor's measurements are known to be relatively free from atmospheric conditions such as rain, fog, and water spray.

As mentioned in the introduction, the sea level measuring standard was changed on 12 December 2007. A sharp offset of about 6.7 m, therefore, was recorded between the data before and after the transition point (TP; see Fig. 2). Before the TP, the range finder recorded the distance from the sensor to the sea surface as sea level. After that, the KHOA altered the standard to record the actual sea level by subtracting the measured distance from the known height from the sea bottom to the sensor (KHOA, 2013). Therefore, this study corrected the forepart by flipping it upside down and then shifting to the position extrapolated to the first time of the data afterward. Also, we performed the harmonic analysis on the corrected SLH time series to validate the correction method. The corrected SLH time series for December 2007 estimated a sufficiently high signal-to-noise ratio (SNR) over 10.0 (Pawlowicz et al., 2002), compared to the much broader ranges like years or decades of SLH at I-ORS. Its consistencies in amplitude and phase with the rear subset also guaranteed the method for correcting the systematic offset.

Table 1. Instrument specifications for the SM-140 by MIROS.

Data	Range	Resolution	Accuracy
Range	1 – 23 m	1 mm	< 5 mm
	3 – 95 m		
Frequency	50 – 200 Hz (according to range)		

https://doi.org/10.5194/egusphere-2024-3380
Preprint. Discussion started: 13 November 2024

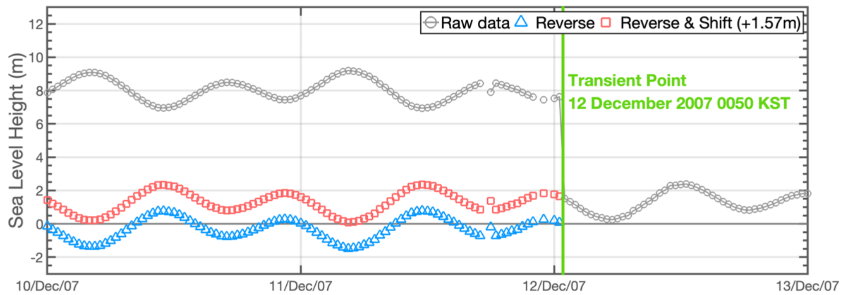

Figure 2. The circle markers indicate each process of methodological adjustment for the data before TP. The grey line with circles means the raw data and blue and red marker lines indicate the reverse and shift (+ 1.57m after reversed) process.

2.1.1 Satellite altimetry and reanalysis products

We collected satellite altimetry and reanalysis datasets to validate the performance of the qualified SLH. The satellite is the gridded L4 sea surface height dataset provided by Copernicus Marine Environment Monitoring Service (CMEMS, https://doi.org/10.48670/moi-00145) for 1993-2022. This altimetry, sea surface height from the geoid, was calculated through optimal interpolation (OI) by merging along-track altimetry from all satellites. Inverted barometric and tidal heights correction was applied to adjust the along-track data. The daily gridded satellite altimetry has a quarter-degree resolution for the global ocean. We used daily SSH time series at the nearest grid point to the I-ORS.

The three SSH products used in this study are the HYbrid Coordinate Ocean Model (HYCOM, https://www.hycom.org/) data-assimilative reanalysis (HYCOM-R) for the period of 2003-2017 and HYCOM non-assimilative simulation (HYCOM-S) from 2018-2022, Global Ocean Physics Reanalysis 12 version 1 (hereafter GLORYS; Lellouche et al., 2021), and the Ocean Reanalysis System 5 (hereafter ORAS5; Zuo et al., 2019). The HYCOM product provided by the Navy's operational Altimeter Processing System (ALPS) has a spatial resolution of 1/12° by 1/12° for the global ocean and a temporal resolution of 3 hourly. GLORYS12 is produced by Mercator Ocean International (https://www.mercator-ocean.fr/en/) and has a spatial resolution of 1/12° by 1/12° for the global ocean with a daily resolution. The ORAS5 provided by the European Center for Medium-Range Weather Forecasts (ECMWF) has a spatial resolution of 1/4° by 1/4° for the global ocean and a temporal resolution of monthly (DOI: 10.24381/cds.67e8eeb7). To efficiently compare sea level variability, the SLH of all datasets was converted to sea level anomalies by subtracting their mean values. Except for ORAS5, which is monthly data, the other sea level data were averaged daily. Similarly, we estimated the daily mean observed time series when more than half of the data were available or flagged as good data.

https://doi.org/10.5194/egusphere-2024-3380
Preprint. Discussion started: 13 November 2024

2.2 TALOD QC

2.2.1 Meta check

After correcting the systematic offset in the observed sea level time series, we classified outliers into four categories: metadata, range, spike, and stuck (see Fig. 3 for a flowchart). The metadata check involves manually flagging unreliable data, including instrumental jolts or a data section that may disrupt the following automatic detection procedures to prevent contamination of the observed data's long-term characteristics. This examination is normally based on historical metadata information (or field notes) on the sensor's maintenance, cleansing, a power shortage event in the ocean research station, etc. Unfortunately, the observed SLH time series from the I-ORS are not distributed with metadata information. Instead, we flagged subjectively a section where the periodicity of SLH data was irregular or nonsensical data existed for several days. For example, from June 2016 to July 2017, the sea level observations at the I-ORS involved two relocations and one replacement of the observational instrument, and the sea levels observed during this period were relatively low (not shown). As a result, 56,024 data points were flagged based on the metadata check accounting for 6.32% of the total observations. This study points out the need for recorded metadata information to ensure quality assessment of the observed time series and efficient instrumental maintenance.

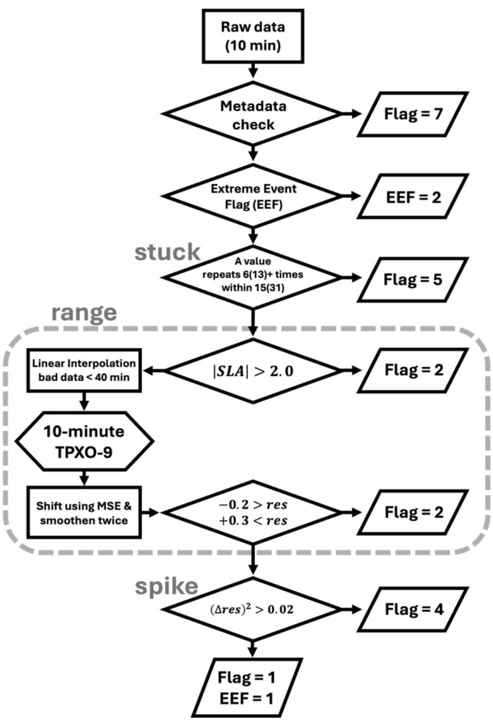

https://doi.org/10.5194/egusphere-2024-3380
Preprint. Discussion started: 13 November 2024

Figure 3. Flow chart of TALOD QC process.

2.2.2 Stuck check

After the metadata check, we recommend examining stuck values in the time series. Generally, a stuck check detects outliers when a fixed value is continuously recorded over a certain period. At the I-ORS, the SLH measurements exhibit two distinct characteristics of stuck values. Firstly, these values persist for a certain duration without variation; a typical QC process can identify this kind of stuck. An abnormal case is observed at the I-ORS: alternation between normal observations (good data) and fixed values. To handle this unusual stuck case efficiently, we adopted the density of identical values over a certain period. We experimented with various range and frequency combinations. As a result, we flagged the cases when a single value was detected more than 6 times within a range of 15 or more than 13 times within a range of 31.

2.2.3 Range check

Normally, range check can be divided into two parts. A local or gross range check designates a single value that is difficult to occur naturally for a target variable at a specific location during the monitoring span. And seasonally varying range check effectively detects errors for variables dominated by seasonal variability, such as air or sea surface temperatures or humidity. However, these methods are not suitable for SLH measurements in shallow water with large tidal amplitudes, such as the maximum tidal amplitude of 2.5 m that can occur at the I-ORS, and significant seasonal cycles (Lee et al., 2006).

This study's range check consists of two procedures: a gross range check with a fixed range by assigning upper (+2.0 m) and lower (–2.0 m) limits for SLA, and a localized check with temporally varying ranges by taking advantage of the tidal prediction model. The gross range check effectively identifies extremely high values such as 29.0 m and 7.98 m, which are frequently recorded in the SLH measurements from the I-ORS even during normal situations. For the local range check, we used the TPXO9 tidal model, which has a 1/30° horizontal resolution. This global tide model offers realistic spatial and temporal tides around the Korean Peninsula with the smallest root mean square difference (RMSD) compared to tide gauge observations (Lee et al., 2022).

Tide data extracted from the TPXO9 sliding every month was adjusted using the observed SLH for the same period (Fig. 4). A month window is selected to consider seasonal evolution. The extracted tidal time series was shifted to positions where the Root Mean Square Errors (RMSEs) are minimized (the red line in Fig. 4). Overshooting tends to be generated when using the arithmetic mean only for the shifting, especially for the convex-up and -down data, which correspond to high and low tides respectively, thus potentially resulting in

https://doi.org/10.5194/egusphere-2024-3380
Preprint. Discussion started: 13 November 2024

detecting overestimated outliers. To address the overshooting issue, the residual time series, i.e., the observations minus mean shifted tides, is smoothed twice and then added to the estimated tidal time series (the green line in Fig. 4). When the difference between the observed SLH and the bias-corrected tide exceeds +0.3 meters or falls below –0.2 meters, the local range check identifies it as an outlier (see Fig. 5b). These thresholds are sufficient for elevation changes associated with nonlinear internal waves in this region (Lee et al., 2006).

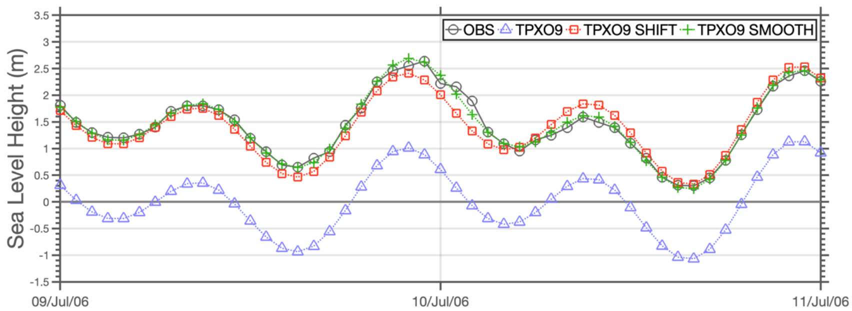

Figure 4. Lines indicate the processes for fitting TPXO9 to observation (black line with circle) in the range check. (1) The blue line with a triangle means raw TPXO9 data. (2) The orange line with the square shows mean-shifted TPXO9 based on the Mean Square Error method. (3) The green line with a circle indicates the final output with a twice-smoothened bias added.

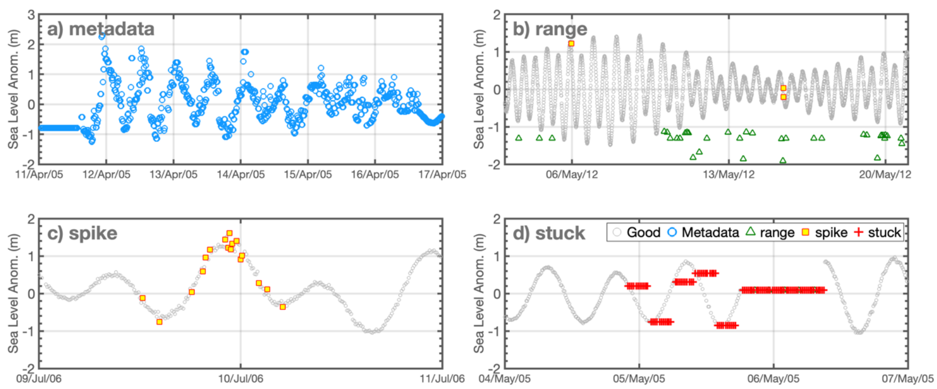

Figure 5. Time series for the examples of 4 flags. a) metadata, b) range, c) spike, and d) stuck. Each marker indicates Good Data (grey circle), metadata (blue circle), range (green triangle), spike (yellow square with red outline), and stuck (red cross), respectively.

2.2.4 Spike check

The spike check is developed based on the Gradient Spike Method (GSM) following Hwang et al. (2022). The GSM generally detects outliers using the gradient of SLH data. However, we employed the temporal discrepancy in the non-tidal residual SLH time series; that is, if the square of that value exceeds 0.02, it is classified as a spike. The equation is as follows:

https://doi.org/10.5194/egusphere-2024-3380
Preprint. Discussion started: 13 November 2024

$$flag = find((\Delta residual)^2 > 0.02), \quad (1)$$

2.2.5 Extreme event flag

Atmospheric factors such as sea level pressure and wind modulate SLH; the inverted barometer effect (IBE) and strong winds can generate abrupt SLH fluctuations. Under extreme weather, the SLH measurements can be classified as an outlier through range and spike checks. The flagged SLH data during severe weather might be regarded as good data, depending on the situation. As a last QC procedure, this study introduced the extreme event flag (EEF) to note that the SLH data was measured over severe weather periods. The typhoon cases analyzed in this study are shown in Table 2.

The observed range of sea surface height anomalies was almost equal for both normal and typhoon situations, i.e., 0.30/–0.20 m and 0.29/–0.20 m, respectively. However, there was a significant difference in variance, which implies large fluctuations in the SLH measurements. The normal case exhibited a variance of 9.0 cm^2, whereas during the typhoon-influenced period, it increased to 40 cm^2, approximately five times higher. Consequently, although the maximum/minimum ranges of residual components remained almost unchanged during typhoon periods, the outliers classified by the spikes increased significantly (Fig. 6). We manually flagged the typhoon period with the EEF based on the daily variance and reported information on typhoons from the KMA.

Table 2. List of Typhoon cases during observation.

Typhoon	Start date	End date
Chanthu (2021)	14 Sep, 2021	16 Sep, 2021
Bavi (2020)	26 Aug, 2020	26 Aug, 2020
Lingling (2019)	6 Sep, 2019	7 Sep, 2019
Kong-rey (2018)	6 Sep, 2018	7 Sep, 2018
Soulik (2018)	22 Aug, 2018	23 Aug, 2018
Chan-hom (2015)	12 Jul, 2015	12 Jul, 2015
Neoguri (2014)	9 Aug, 2014	9 Aug, 2014
Bolaven (2012)	27 Aug, 2012	28 Aug, 2012
Muifa (2011)	8 Aug, 2011	9 Aug, 2011
Megi (2004)	10 Aug, 2004	10 Aug, 2004

https://doi.org/10.5194/egusphere-2024-3380
Preprint. Discussion started: 13 November 2024

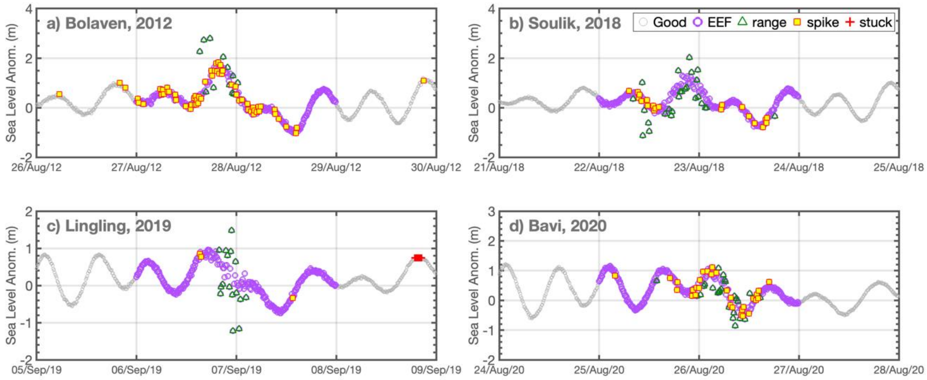

Figure 6. Same as Fig. 5, but for Typhoon cases.

3 results

3.1 Comparative analysis to existing QC process

Representative results obtained during the TALOD QC are shown in Figure 7, and the number of outliers and proportions flagged by each QC process are presented in Table 3. The results were compared with those obtained by applying the IOC's standard QC process to assess the performance of the TALOD QC process. The IOC was designed and applied as a QC procedure consisting of several steps to accord with international standards through the support of the National Data Buoy Center (NDBC) and the National Science Foundation under the National Oceanic and Atmospheric Administration (NOAA) to provide uniformly qualified observations to scientists (Min et al., 2020). The differences between those two QC processes are illustrated in Figure 8 and summarized in Table 4.

We collected a total of 1,011,584 SLH data observed at I-ORS during the observation period from 2003 to 2022. After excluding 165,702 instances of missing values (NaNs), 886,128 data points were kept for quality control and analysis. Of these, 793,034 (89.49%) were classified as good data, while 93,184 data points (10.51%) were flagged as bad through the TALOD QC procedure (Table 3). Among the flagged data, excluding those flagged as the meta, stuck values constituted the majority, representing 89.84% of the bad data. This was followed by spike and range flags, accounting for 5.52% and 4.64% of the bad data, respectively.

Seasonal patterns in the frequency of each flag were further analyzed. The number of occurrences of bad data was found to be the highest in spring, exceeding the annual average by a factor of 1.28. This seasonal increase was primarily driven by a higher occurrence rate of stuck errors. Specifically, a total of 33,383 stuck errors were

https://doi.org/10.5194/egusphere-2024-3380
Preprint. Discussion started: 13 November 2024

recorded, with 16,536 instances occurring in spring, the highest count across all seasons (winter: 5,795; summer: 7,985; autumn: 3,067). The spring frequency of stuck errors was nearly double the annual average (1.98 times). Other bad data types, such as range and spike, exhibited relatively low frequencies throughout the whole season, with total counts of 1,725 and 2,052, respectively. Conversely, the meta-flagged data, which accounted for the largest proportion of bad data excluding NaN values, displayed a uniform distribution across all seasons, with a mean of 56,024 occurrences (winter: 14,934; spring: 12,298; summer: 14,843; autumn: 13,949). As a result, the meta flag did not contribute significantly to the observed seasonal variations in the long-term perspective.

The overshooting-like errors related to extreme weather conditions, such as range and spike flags showed peak occurrence rates in summer. This seasonal pattern coincided with the peak typhoon season over the NWP, indicating a linkage between extreme weather events and the occurrence of overshooting-like error types.

The SLH is dominated by neap-spring tidal cycles, and it can induce misclassifications in error detection by a range check that adopts a constant value as a threshold. However, the TALOD method utilizes residual components that consider the rapid increase/decrease of SLH caused by most diurnal components and short-duration weather systems, thereby reducing detection errors. For example, the range check in the TALOD QC process successfully flagged 1,936 data points by outliers. In detail, the gross range check detected 1,121 bad data, while the temporal and local outlier detection identified 815 instances of bad data. As a result, the temporally and locally utilized outlier detection method successfully captured the errors with little biases. The TALOD QC process preemptively flags bad data that excessively disrupt continuity through the range checks. This approach, as depicted in Figure 8f, prevents detection failures caused by recurrent spike error values. The IOC's spike check has trouble with flagging spike-type errors within a short period. These unqualified outlying values may provoke the downgrading in the performance of the spike check using min/max for calculating threshold. Attention should be given when applying the IOC QC processes to such sea level measurements because the automatic QC on observation data could be vulnerable to recurrently recorded spike-like errors. For instance, among the 261 observations logged from 1 June 2016 00 KST to 14 June 2016 00 KST, the TALOD method flagged 43 instances as bad data, while IOC identified 37 values only with apparent error-like values still remaining (see Fig. 8e and 8f).

Moreover, as summarized in Table 4, the two QC processes showed significant differences in the stuck check. While the TALOD QC process successfully detects stuck values, as illustrated in Figure 8a, 8c, 8e, and 8g, the IOC seems to fail to identify these error-like values. Instead of flagging abnormal stuck values, the IOC QC removes the entire section (Fig. 8b, 8d, 8f, and 8h). Furthermore, the IOC's stuck check, which is designed to identify values as stuck when the sensor records the same values, tends to classify excessively normal data into stuck errors due to instrumental issues including low frequency (10 minutes); these situations are frequently observed during high and leap tides (Fig. 8d).

During the application of the IOC Process to SLH data, misclassifications or detection failures were confirmed due to the inability to identify irregularly repeated stuck errors. However, the TALOD applied optimized detection techniques, and 45,850 stuck errors were successfully flagged. Figure 9 shows the distribution of observed and qualified SLAs. Compared to the idealized normal distribution indicated by the grey line in Figure 9, unusually high values were concentrated in the ranges of –1.4 to –1.3 m, –0.2 to –0.1 m, and 0.4 to 0.5 m. After the TALOD QC, this distribution is more closely aligned with the normal distribution, indirectly suggesting the performance of the TALOD QC to identify outliers.

Table 3. Detection counts and proportions for each flag from Oct 2003 to Dec 2022 (excluding NaN values).

Flag number	**1**	**2**	**4**	**5**	**7**	**8**
(Name)	**(Good data)**	**(Range)**	**(Spike)**	**(Stuck)**	**(Metadata)**	**(NaN)**
#	793,034	1,725	2,052	33,383	56,024	165,702
% (without NaN)	89.49%	0.19%	0.23%	3.77%	6.32%	

Table 4: The differences in flag detection methods between TALOD and IOC.

Flag	**TALOD**	**IOC**
Range	Data point where observation exceeds the threshold from the tidal component, which is adjusted according to temporal observations	Data point exceeds sensor or operator-selected min/max for whole period
SPIKE	Data point where the square of the difference in residuals exceeds the threshold	Data point n-1 exceeds a selected threshold relative to adjacent data points
STUCK	Data point where the reoccurrence rates for constant value within the windows are over thresholds	Invariant value

https://doi.org/10.5194/egusphere-2024-3380
Preprint. Discussion started: 13 November 2024

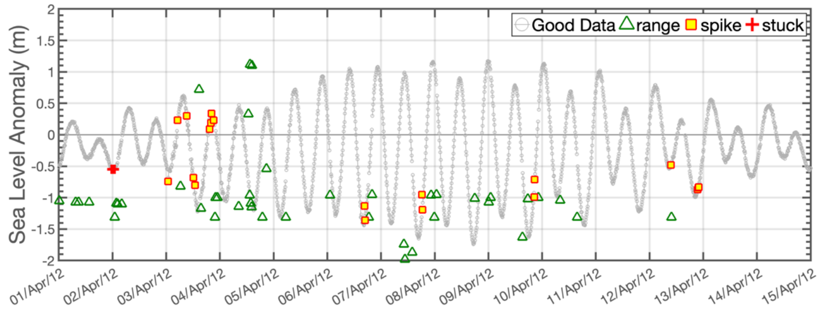

Figure 7. Representative results from 01 Apr 2012 to 15 Apr 2012

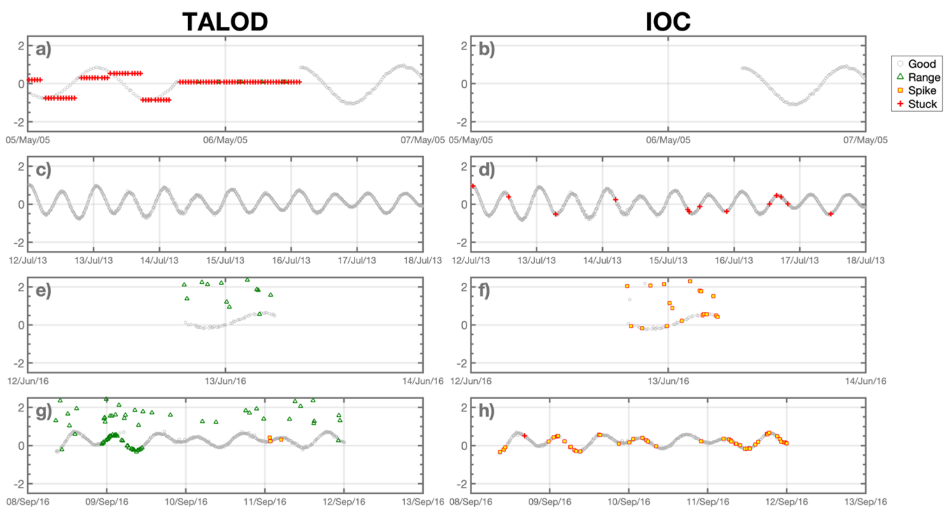

Figure 8. Same as Fig. 5, but for invariant stuck case (a-b, from 05 May 2005 to 07 May 2005), stuck case during short-period (c-d, from 12 Jul 2013 to 18 Jul 2013), range-spike misclassification case (e-f, from 12 Jun 2016 to 14 Jun 2016), and range-spike mixed case (g-h, 08 Sep 2016 to 13 Sep 2016). The figures on the left and right sides show results for TALOD and IOC, respectively.

https://doi.org/10.5194/egusphere-2024-3380
Preprint. Discussion started: 13 November 2024

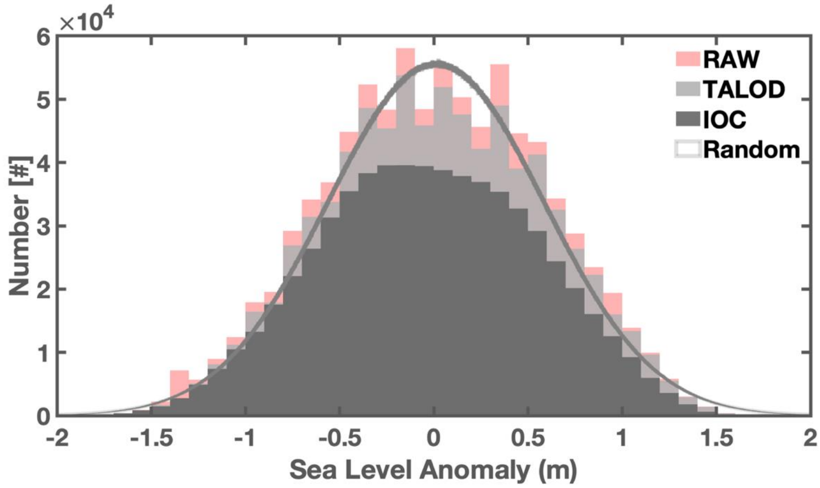

Figure 9. Histogram of observed sea level anomaly without QC (light red) and with QC (light grey) from 2003 to 2022 at I-ORS. the area enclosed by a darker grey line indicates the normal distribution.

3.2 Data validation by using observation data

Figure 10 displays the daily time series of SLA for each dataset except ORAS5. SLH generally represents the vertically integrated heat contents of the ocean. Therefore, there are higher SLAs during the boreal summer period, June-September, and lower SLAs during the boreal winter, December-March. The daily mean sea level range is approximately ± 0.6 m for the observed one, –0.4 to +0.6 for the HYCOM product, and ± 0.3 m for GLORYS and satellite altimetry. We calculated the standard deviation (STD) and variance of each dataset to infer their variability and distribution. The STD and variance for the I-ORS measurements were 0.16 m and 0.02 m, respectively. For satellite and GLORYS, the values were the same at 0.10 m and 0.01 m. The HYCOM-R had values of 0.11m and 0.01m. Both Satellite and the two reanalysis data simulated lower variability of SLH compared to the in-situ observation. However, both datasets captured the overall pattern well, showing high accuracy with a low RMSE of less than 0.1m. Compared to HYCOM, which has a spatial resolution of 1/12° and a temporal resolution of 3-hourly, the satellite exhibits lower seasonal variance, which might be due to substantial optimal interpolation procedure to reduce high-frequency noise during a gridding process. Besides, significant statistical differences were found between HYCOM and other datasets (OBS and reanalysis data) for the period after 2018. Therefore, we further analyzed the HYCOM data by dividing it into two periods: before 2018 (HYCOM-R) and after 2018 (HYCOM-S).

First, we compared the SLR rates of each dataset (Fig. 10). The observation exhibited a SLR of 5.27 mm/yr for this period from 2003 to 2022, while the satellite altimetry rendered slightly lower rates of 2.76 mm/yr. Owing to

https://doi.org/10.5194/egusphere-2024-3380
Preprint. Discussion started: 13 November 2024

a robust falling trend in the HYCOM's SLA during the recent period since 2018 (–24.42 mm/yr; HYCOM-S), the overall rate of SLR for the HYCOM was negative (–4.22 mm/yr) during the study period, but the HYCOM-R has a 2.70 mm/yr trend from 2003 to 2017. This result might indicate that we must be careful when using the HYCOM-R and HYCOM-S products to study long-term climate dynamics.

Figure 11a shows the monthly sea level trends for the observation and other four datasets. The observation showed a higher sea level rise rate (5.27±0.46 mm/yr) compared to the other datasets. ORAS5 exhibited a trend similar to satellite altimetry, while GLORYS and HYCOM showed a sea level fall trend. As mentioned earlier, HYCOM showed a strong fall trend unlike other datasets because it simulated lower sea levels after 2018. Also, we compared the correlation and variability between the observation and the other four datasets using a Taylor Diagram (Fig. 11b). Satellite altimetry exhibited the highest accuracy among the datasets, with a high correlation coefficient (0.71) and low RMSE (0.04 m) compared to the observation. For HYCOM, it showed the lowest correlation coefficient (-0.08) and highest RMSE (0.10 m) over the entire period, indicating poor agreement. HYCOM-R demonstrated performance close to Satellite, whereas HYCOM-S exhibited a significantly low correlation coefficient (-0.39) and high RMSE (0.12 m). The correlation coefficients of ORAS5 and GLORYS were 0.71 and 0.76, respectively, and the RMSE of both data was 0.1 m, showing higher correlation and accuracy than HYCOM. HYCOM was found to have an overall lower performance due to its inability to simulate the variability of SLH since 2018 in HYCOM-S.

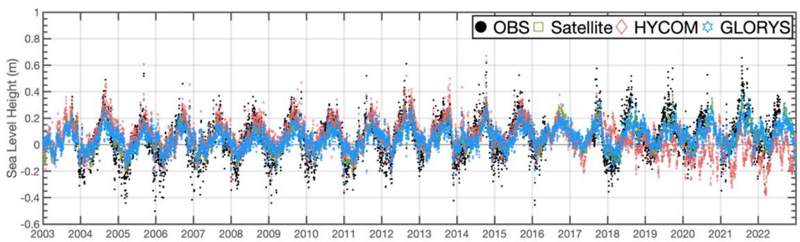

Figure 10. Time series of monthly QC-ed observations (black dot), Satellite (green empty circle), HYCOM (light red diamond), and GlORYS12 (light cyan hexagram) data during the observation period at the I-ORS.

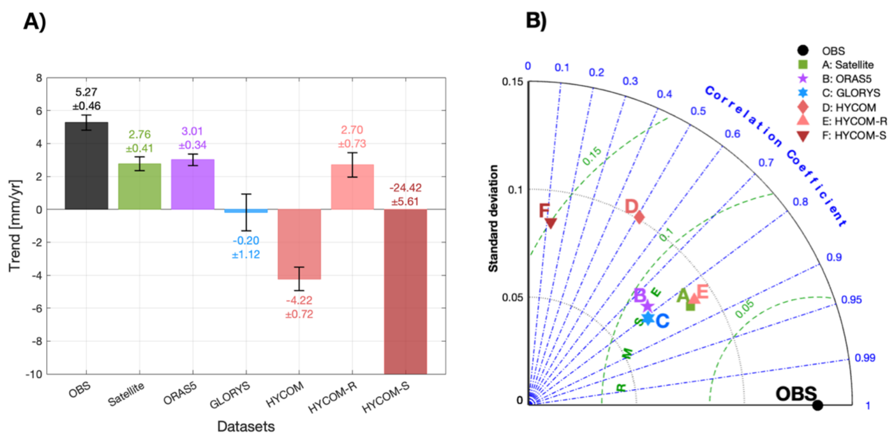

Figure 11. Bar plot with error bar (A; Left) and Modified Taylor diagram (B; Right). the azimuthal angle represents the correlation coefficient, the radial distance indicates the standard deviation, and the semicircles centered at the "OBS" marker mean the Root Mean Square Errors. The colors and markers indicate each data (black circle: observation, green square: Satellite, light cyan hexagram: GLORYS, purple pentagram: ORAS5, red diamond: HYCOM, light red upward-pointing triangle: HYCOM-R, light red downward-pointing triangle: HYCOM-S).

3.3 Sea-level budget assessment at I-ORS

As mentioned above, the SLH of the I-ORS produced through the developed QC process estimated a SLR rate of 5.27±0.46 mm/yr. Sea level change is divided into relative and geocentric sea level change representing the distance from the sea floor and center of the earth to the sea surface, respectively. The ground-based observations such as I-ORS are relative sea level. and its change can be affected by various physical processes including sea level change due to ocean density and circulation (sterodynamic effect), mass exchange between the ocean and land (barystatic effect), glacial isostatic adjustment (GIA) (Gregory et al., 2019; Frederikse et al., 2020; Cha et al., 2024). In this regard, we performed a budget analysis of each physical process affecting SLR at the I-ORS.

The sterodynamic (SD) effect is calculated as the sum of dynamic sea level change (DSL) and global mean steric sea level rise (GMSSL) (Gregory et al., 2019). DSL was obtained from ORAS5, which was also used for validation data in this study. GMSSL used in-situ observation data provided by the Institute of Atmospheric Physics (IAP, Cheng et al., 2017), Met Office Hadley Centre (EN4, Good et al., 2013), and Japan Meteorological Agency (JMA, Ishii et al., 2017). GMSSL was produced using the temperature-salinity profile data from each institution and was used to compute the SD effect by adding the DSL. The barystatic (BS) effect is the sum of ice melting from the Antarctica, and Greenland ice sheets, glaciers, and changes in land water storage. Here, we used ocean mass reconstructed barystatic data from Ludwigsen et al. (2024). GIA comprises sea level changes due to the disappearance of glaciers since the glacial period, and we took the model results from Caron et al. (2018). Caron et al. (2018) utilized a global positioning system (GPS) time series from 459 sites and 11,451 relative sea level data to improve the model accuracy, and based on this, computed the ensemble mean of 128,000 model simulation results.

Figure 12 shows the sea level time series and trend budget at the I-ORS along with a comparison to satellite altimetry. The sea level change rate due to physical processes (Sum=SD+BS+GIA) was 2.57±0.35 mm/yr, about 2.70±0.58 smaller than the observation (5.27±0.46 mm/yr). This discrepancy was also found in comparing satellite altimetry and observation (diff: 2.51±0.62 mm/yr). Among the components for physical processes, SD contributed 0.73±0.34 mm/yr, approximately 28% of the rise. The BS effect had the largest contribution, at 1.85±0.02 mm/yr (about 72%). Meanwhile, GIA led to a slight fall in sea level, contributing -0.11±0.00 mm/yr, about 0.04%.

Satellites cannot detect vertical land motion (VLM) because they measure the change in distance from the center of the earth to the sea surface, whereas station observations such as I-ORS are affected by VLM because they measure the change in height from the sea floor to sea level (Han et al., 2014; Gregory et al., 2019; Cha et al., 2024).Thus the difference between the sea level trend from satellite altimetry and I-ORS can be regarded as VLM component, we checked whether a difference of approximately 2.51±0.62 mm/yr was associated with VLM. Cha et al. (2024) defined the total VLM as the sum of the VLM components in GIA, BS, and local processes, where GIA and BS are categorized as natural processes. The VLM of GIA was obtained from Caron et al. (2018), the VLM of BS used the data of Frederikse et al. (2020), and the VLM component of the local process was calculated using the difference between sea level change due to physical processes (2.57±0.35 mm/yr) and sea level change from observation (5.27±0.46 mm/yr). At the I-ORS location, the VLM of GIA was calculated to be 0.22±0.14 mm/yr, the VLM of BS was 0.28±0.64 mm/yr, and the VLM of the local process was –2.67±0.60 mm/yr. Therefore, the total VLM was approximately –2.17±0.89 mm/yr, indicating significant ground subsidence at the I-ORS location, and this subsidence was more affected by local processes than by natural effects such as GIA and BS.

Additionally, we analyzed the trend of observed vertical displacements using the Global Navigation Satellite System (GNSS) observing 30-second intervals at the I-ORS from 2013 to 2019. The trend of GNSS vertical displacements was –0.89±0.47 mm/yr, using daily mean. it's smaller than the VLM of the local process (2.67±0.60 mm/yr), but it certified that the actual ground subsidence exists.

https://doi.org/10.5194/egusphere-2024-3380
Preprint. Discussion started: 13 November 2024

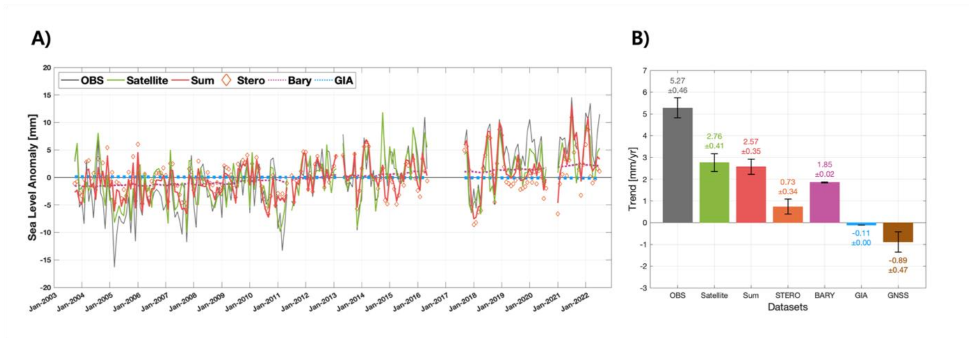

Figure 12. Monthly time series of sea level anomalies (left) and bar chart with error bar for sea level rise rate (right; units: mm/yr). Each color and type of line indicates the dataset (OBS: black solid line, Satellite: green solid line, Sum: bright red solid line, STERO: orange diamond, BARY: purple dotted line, GIA: sky-blue dotted line, and GNSS: bright brown).

4 Summary and Discussion

This study developed a novel quality control procedure based on a high-resolution tidal prediction model, named the Temporally and Locally Optimized Detection (TALOD) method, and applied it to 10-minute interval real-time SLH data observed by the MIROS Range Finder (SM-140) from 2003 to 2022. The TALOD method is divided into manual and automatic processes. The manual process includes a METADATA check that relies on the empirical knowledge of the data producer. The METADATA check flags sections that could contaminate the long-term characteristics of the collected time series observations. This check improves the performance of subsequent automatic QC processes. The automatic process includes RANGE, SPIKE, and STUCK checks. The range check with residual components derived from the tidal prediction model, TPXO9, may enable it to address known issues such as detection failure due to non-periodic outliers or adulteration when estimating the tidal components using the least square method. Spatiotemporally optimized thresholds reduce misclassification and detection failures caused by frequent error values during the spike check. The spike check detected bad data by setting a spatially and temporally optimized threshold using the non-tidal residual component. This approach can reduce false detections compared to the gradient-based GSM. Also, the GSM method tends to detect rapidly fluctuating SLH, such as extreme weather events, as an outlier. In the stuck check, we also utilized the occurrence frequency of specific values to handle the alternating of the good and bad data, the unique characteristics in SLH at the I-ORS. This study confirmed that a novel stuck check using the reoccurrence rate of the same value for a specific period can reduce truncation and increase the retention rate of good data compared to existing QC processes such as IOC.

https://doi.org/10.5194/egusphere-2024-3380
Preprint. Discussion started: 13 November 2024

To evaluate the reliability of SLH data applying the TALOD and analyze the characteristics of SLH data from various institutions, we collected and compared with HYCOM, Satellite, GLORYS, and ORAS5. Before 2018, HYCOMa and Satellite data exhibited the highest performance, while GLORYS and ORAS5 showed relatively higher RMSE. Since 2018, the trend of SLH for HYCOM (HYCOMb) was –23.86 mm/yr, which showed unrealistic results compared to other datasets. In conclusion, the reanalysis data, including HYCOMa and satellite altimetry, showed a more similar pattern to the observation, and the others exhibited a quite narrower distribution for anomalies. Through assessment, we confirmed an issue with the variability of SLH in HYCOM, and the reliability and validity of the TALOD QC method and SLH observation at I-ORS.

The TALOD QC process includes the extreme event flag (EEF), which indicates the period during which SLH is affected by extreme weather. For instance, since the variance of SLH was more than four times larger (including flagged data) than usual during the typhoon-influenced period, some good data can be flagged as range and spike errors. Ensuring sufficient observation numbers is crucial for research on typhoons. Therefore, we provide the extreme event option so researchers can use these data for extreme weather dynamics.

In the budget analysis, the BS effect related to mass exchange between the ocean and land contributed significantly, accounting for approximately 70% of the total sea level change. The difference in sea level trend between the I-ORS and satellite altimetry (about 2.67 mm/yr) was attributed to VLM. The total VLM estimated from reanalysis data (-2.17 mm/yr) indicates considerable ground subsidence at the I-ORS site. In detail, this subsidence was more influenced by local processes than natural processes such as BS or GIA. Although the total VLM varies depending on the reanalysis data, the GNSS-measured vertical displacement trend from 2013 to 2019 was calculated at -0.89±0.47 mm/yr, demonstrating the ongoing ground subsidence at the I-ORS.

Despite the advancements in the TALOD QC process, several challenges remain. The TALOD QC process only targets the observed SLH and is still not fully automated. Additionally, there is a need for further processes that make it possible to take count of misclassification in extreme weather, such as rogue waves. In normal cases, good data with extreme values induced by the inverted barometer and steric effect may be erroneously identified as errors. Thus, an additional step of adjusting coefficients using atmospheric and oceanographic observation variables is required.

Nevertheless, the TALOD QC process has the utility of being applied to both tide gauges and range finders. It also utilizes predicted tidal components for each point, enhancing its adaptability. Well-controlled in-situ data are essential not only for data assimilation and validation but also for data management. The I-ORS platform stands out as a unique resource, offering over 20 years of continuous atmospheric and oceanographic observation data in the open sea. Additionally, the Gageocho Ocean Research Station (G-ORS) and Socheongcho Ocean Research Station (S-ORS) are positioned along the meridian, contributing to the study of marine environmental development.

Acknowledgement

This research was supported by Korea Institute of Marine Science & Technology Promotion (KIMST) funded by the Ministry of Oceans and Fisheries (RS-2021-KS211502 and RS-2022-KS221544), and by the Korea Institute of Ocean Science & Technology (PEA0201).

Author contributions

Taek-bum Jeong: Conceptualization, Methodology, Formal analysis, Writing – original draft, Writing – review & editing. Yong Sun Kim: Conceptualization, Methodology, Validation, Writing – review & editing, second contact author. Hyeosoo Cha: Conceptualization, Methodology, Validation, Writing – review & editing. Kwang-Young Jeong: Conceptualization, Methodology, Writing – review & editing. Mi-Jin Jang: Conceptualization, Methodology, Writing – review & editing. Jin-Yong Jeong: Conceptualization, Methodology, Writing – review & editing. Jae-Ho Lee: Conceptualization, Methodology, Validation, Writing – review & editing, first contact author.

Competing interests

The contact author has declared that none of the authors has any competing interests.

Special issue statement

This article is part of the special issue "Oceanography at coastal scales: modelling, coupling, observations, and applications".

Acknowledgements

This research was supported by Korea Institute of Marine Science & Technology Promotion (KIMST) funded by the Ministry of Oceans and Fisheries (RS-2021-KS211502 and RS-2022-KS221544), and by the Korea Institute of Ocean Science & Technology (PEA0201).

https://doi.org/10.5194/egusphere-2024-3380
Preprint. Discussion started: 13 November 2024

References

Calafat, F. M., Wahl, T., Tadesse, M. G., and Sparrow, S. N.: Trends in Europe storm surge extremes match the rate of sea-level rise, Nature, 603, 841-845, 2022. a

Caron, L., Ivins, E., Larour, E., Adhikari, S., Nilsson, J., and Blewitt, G.: GIA model statistics for GRACE hydrology, cryosphere, and ocean science, Geophysical Research Letters, 45, 2203-2212, 2018. a, b, c

Cayan, D. R., Bromirski, P. D., Hayhoe, K., Tyree, M., Dettinger, M. D., and Flick, R. E.: Climate change projections of sea level extremes along the California coast, Climatic Change, 87, 57-73, 2008. a

Cazenave, A., Meyssignac, B., Ablain, M., Balmaseda, M., Bamber, J., Barletta, V., Beckley, B., Benveniste, J., Berthier, E., and Blazquez, A.: Global sea-level budget 1993-present, 2018. a

Cha, H., Moon, J.-H., Kim, T., and Song, Y. T.: A process-based assessment of the sea-level rise in the northwestern Pacific marginal seas, Communications Earth & Environment, 4, 300, 2023. a, b

Cha, H., Jo, S., and Moon, J.-H.: A Process-based Relative Sea-level Budget Along the Coast of Korean Peninsula Over 1993–2018, Ocean and Polar Research, 46, 31-42, 2024. a, b, c

Chen, X., Zhang, X., Church, J. A., Watson, C. S., King, M. A., Monselesan, D., Legresy, B., and Harig, C.: The increasing rate of global mean sea-level rise during 1993–2014, Nature Climate Change, 7, 492-495, 2017. a, b

Cheng, L., Trenberth, K. E., Fasullo, J., Boyer, T., Abraham, J., and Zhu, J.: Improved estimates of ocean heat content from 1960 to 2015, Science Advances, 3, e1601545, 2017. a

Dieng, H. B., Cazenave, A., Meyssignac, B., and Ablain, M.: New estimate of the current rate of sea level rise from a sea level budget approach, Geophysical Research Letters, 44, 3744-3751, 2017. a

Erofeeva, S. and Egbert, G. D.: TPXO9–a new global tidal model in TPXO series, 2018 Ocean Sciences Meeting, 2018. a

Fox-Kemper, B., Hewitt, H., Xiao, C., Aðalgeirsdóttir, G., Drijfhout, S., Edwards, T., Golledge, N., Hemer, M., Kopp, R., and Krinner, G.: Ocean, cryosphere and sea level change. Climate change 2021: the physical science basis. Contribution of Working Group I to the Sixth Assessment Report of the Intergovernmental Panel on Climate Change, P. Zhai, editor;, A. Pirani, editor, 2021. a

Frederikse, T., Landerer, F., Caron, L., Adhikari, S., Parkes, D., Humphrey, V. W., Dangendorf, S., Hogarth, P., Zanna, L., and Cheng, L.: The causes of sea-level rise since 1900, Nature, 584, 393-397, 2020. a, b

Good, S. A., Martin, M. J., and Rayner, N. A.: EN4: Quality controlled ocean temperature and salinity profiles and monthly objective analyses with uncertainty estimates, Journal of Geophysical Research: Oceans, 118, 6704-6716, 2013. a

Gregory, J. M., Griffies, S. M., Hughes, C. W., Lowe, J. A., Church, J. A., Fukimori, I., Gomez, N., Kopp, R. E., Landerer, F., and Cozannet, G. L.: Concepts and terminology for sea level: Mean, variability and change, both local and global, Surveys in Geophysics, 40, 1251-1289, 2019. a, b, c

Ha, K.-J., Nam, S., Jeong, J.-Y., Moon, I.-J., Lee, M., Yun, J., Jang, C. J., Kim, Y. S., Byun, D.-S., and Heo, K.-Y.: Observations utilizing Korea ocean research stations and their applications for process studies, Bulletin of the American Meteorological Society, 100, 2061-2075, 2019. a

Hamlington, B. D., Gardner, A. S., Ivins, E., Lenaerts, J. T., Reager, J., Trossman, D. S., Zaron, E. D., Adhikari, S., Arendt, A., and Aschwanden, A.: Understanding of contemporary regional sea-level change and the implications for the future, Reviews of Geophysics, 58, e2019RG000672, 2020. a

Han, G., Ma, Z., Bao, H., and Slangen, A.: Regional differences of relative sea level changes in the Northwest Atlantic: Historical trends and future projections, Journal of Geophysical Research: Oceans, 119, 156-164, 2014. a

Hwang ,Y., Do, K., Jeong, J., Lee, E., and Shin, S.: Algorithm Development for Quality Control of RangeFinder Wave Time Series Data at Ocean Research Station, Journal of Coastal Disaster Prevention, 9, 171-178, 2022. a

Ishii, M., Fukuda, Y., Hirahara, S., Yasui, S., Suzuki, T., and Sato, K.: Accuracy of global upper ocean heat content estimation expected from present observational data sets, Sola, 13, 163-167, 2017. a

Jean-Michel, L., Eric, G., Romain, B.-B., Gilles, G., Angélique, M., Marie, D., Clément, B., Mathieu, H., Olivier, L. G., and Charly, R.: The Copernicus global 1/12 oceanic and sea ice GLORYS12 reanalysis, Frontiers in Earth Science, 9, 698876, 2021. a

KHOA (Korea Hydrographic and Oceanographic Agency): Analysis and Prediction of Sea Level Change, 2013.

Kim, D.-Y., Park, S.-H., Woo, S.-B., Jeong, K.-Y., and Lee, E.-I.: Sea level rise and storm surge around the southeastern coast of Korea, Journal of Coastal Research, 239-243, 2017. a

Kim, Y. S., Jang, C. J., Noh, J. H., Kim, K.-T., Kwon, J.-I., Min, Y., Jeong, J., Lee, J., Min, I.-K., and Shim, J.-S.: A Yellow Sea monitoring platform and its scientific applications, Frontiers in Marine Science, 6, 601, 2019. a

Kim, G.-U., Lee, K., Lee, J., Jeong, J.-Y., Lee, M., Jang, C. J., Ha, K.-J., Nam, S., Noh, J. H., and Kim, Y. S.: Record-breaking slow temperature evolution of spring water during 2020 and its impacts on spring bloom in the Yellow Sea, Frontiers in Marine Science, 9, 824361, 2022. a

Kim, G.-U., Oh, H., Kim, Y. S., Son, J.-H., and Jeong, J.-Y.: Causes for an extreme cold condition over Northeast Asia during April 2020, Scientific Reports, 13, 3315, 2023a. a

https://doi.org/10.5194/egusphere-2024-3380
Preprint. Discussion started: 13 November 2024

Kim, G.-U., Lee, J., Kim, Y. S., Noh, J. H., Kwon, Y. S., Lee, H., Lee, M., Jeong, J., Hyun, M. J., and Won, J.: Impact of vertical stratification on the 2020 spring bloom in the Yellow Sea, Scientific reports, 13, 14320, 2023b. a

Kim, K.-Y. and Kim, Y.: A comparison of sea level projections based on the observed and reconstructed sea level data around the Korean Peninsula, Climatic Change, 142, 23-36, 2017. a

Kulp, S. A. and Strauss, B. H.: New elevation data triple estimates of global vulnerability to sea-level rise and coastal flooding, Nature Communications, 10, 1-12, 2019. a

Lee, J. H., Lozovatsky, I., Jang, S. T., Jang, C. J., Hong, C. S., and Fernando, H.: Episodes of nonlinear internal waves in the northern East China Sea, Geophysical research letters, 33, 2006. a, b

Lee, K., Nam, S., Cho, Y.-K., Jeong, K.-Y., and Byun, D.-S.: Determination of long-term (1993–2019) sea level rise trends around the korean peninsula using ocean tide-corrected, multi-mission satellite altimetry data, Frontiers in Marine Science, 9, 810549, 2022. a, b

Li, Y., Feng, J., Yang, X., Zhang, S., Chao, G., Zhao, L., and Fu, H.: Analysis of sea level variability and its contributions in the Bohai, Yellow Sea, and East China Sea, Frontiers in Marine Science, 11, 1381187, 2024. a

Ludwigsen, C. B., Andersen, O. B., Marzeion, B., Malles, J.-H., Müller Schmied, H., Döll, P., Watson, C., and King, M. A.: Global and regional ocean mass budget closure since 2003, Nature Communications, 15, 1416, 2024. a

Min, Y., Jeong, J.-Y., Jang, C. J., Lee, J., Jeong, J., Min, I.-K., Shim, J.-S., and Kim, Y. S.: Quality Control of Observed Temperature Time Series from the Korea Ocean Research Stations: Preliminary Application of Ocean Observation Initiative's Approach and Its Limitation, Ocean and Polar Research, 42, 195-210, 2020. a, b, c

Min, Y., Jun, H., Jeong, J.-Y., Park, S.-H., Lee, J., Jeong, J., Min, I., and Kim, Y. S.: Evaluation of International Quality Control Procedures for Detecting Outliers in Water Temperature Time-series at Ieodo Ocean Research Station, Ocean and Polar Research, 43, 229-243, 2021. a

Moon, I.-J., Shim, J.-S., Lee, D. Y., Lee, J. H., Min, I.-K., and Lim, K. C.: Typhoon researches using the Ieodo Ocean Research Station: Part I. Importance and present status of typhoon observation, Atmosphere, 20, 247-260, 2010. a

Nerem, R. S., Beckley, B. D., Fasullo, J. T., Hamlington, B. D., Masters, D., and Mitchum, G. T.: Climate-change–driven accelerated sea-level rise detected in the altimeter era, Proceedings of the national academy of sciences, 115, 2022-2025, 2018. a

https://doi.org/10.5194/egusphere-2024-3380
Preprint. Discussion started: 13 November 2024

OOI: Protocols and procedures for OOI data products: QA, QC, calibration, physical samples, version 1-22. Consortium for Ocean Leadership, https:// oceanobservatories.org/wp-content/uploads/2015/09/1102-00300_Protocols_Procedures_Data_Products_QAQC_Cal _Physical_Samples_OOI, Accessed 30 Sep 2019, 2013. a

Park, J. H., Yeo, D. E., Lee, K., Lee, H., Lee, S. W., Noh, S., Kim, S., Shin, J., Choi, Y., and Nam, S.: Rapid decay of slowly moving Typhoon Soulik (2018) due to interactions with the strongly stratified northern East China Sea, Geophysical Research Letters, 46, 14595-14603, 2019. a

Pawlowicz, R., Beardsley, B., and Lentz, S.: Classical tidal harmonic analysis including error estimates in MATLAB using T_TIDE, Computers & geosciences, 28, 929-937, 2002. a

Pirooznia, M., Rouhollah Emadi, S., and Najafi Alamdari, M.: Caspian Sea tidal modelling using coastal tide gauge data, Journal of Geological Research, 2016, 6416917, 2016. a

Pörtner, H.-O., Roberts, D. C., Masson-Delmotte, V., Zhai, P., Tignor, M., Poloczanska, E., and Weyer, N.: The ocean and cryosphere in a changing climate, IPCC special report on the ocean and cryosphere in a changing climate, 1155, 10.1017, 2019. a

Pugh, D.: Tides, Surges and Mean Sea-Level. John Wiley and sons, Bath Typesetting Limited, Great Britain, 555, 1987. a

Pytharouli, S., Chaikalis, S., and Stiros, S. C.: Uncertainty and bias in electronic tide-gauge records: Evidence from collocated sensors, Measurement, 125, 496-508, 2018. a

Roemmich, D., Gilson, J., Davis, R., Sutton, P., Wijffels, S., and Riser, S.: Decadal spinup of the South Pacific subtropical gyre, Journal of Physical Oceanography, 37, 162-173, 2007. a

Royston, S., Dutt Vishwakarma, B., Westaway, R., Rougier, J., Sha, Z., and Bamber, J.: Can we resolve the basin-scale sea level trend budget from GRACE ocean mass?, Journal of Geophysical Research: Oceans, 125, e2019JC015535, 2020. a

Saranya, J., Dasgupta, P., and Nam, S.: Interaction between typhoon, marine heatwaves, and internal tides: Observational insights from Ieodo Ocean Research Station in the northern East China Sea, Geophysical Research Letters, 51, e2024GL109497, 2024. a

Yang, S., Moon, I.-J., Bae, H.-J., Kim, B.-M., Byun, D.-S., and Lee, H.-Y.: Intense atmospheric frontogenesis by air–sea coupling processes during the passage of Typhoon Lingling captured at Ieodo Ocean Research Station, Scientific Reports, 12, 15513, 2022. a

https://doi.org/10.5194/egusphere-2024-3380
Preprint. Discussion started: 13 November 2024

Yin, J., Griffies, S. M., Winton, M., Zhao, M., and Zanna, L.: Response of storm-related extreme sea level along the US Atlantic coast to combined weather and climate forcing, Journal of Climate, 33, 3745-3769, 2020. a

Zuo, H., Balmaseda, M. A., Tietsche, S., Mogensen, K., and Mayer, M.: The ECMWF operational ensemble reanalysis–analysis system for ocean and sea ice: a description of the system and assessment, Ocean science, 15, 779-808, 2019. a

https://doi.org/10.5194/egusphere-2024-3380
Preprint. Discussion started: 13 November 2024

List of Table

Table 1. Instrument specifications for the SM-140 by MIROS.

Table 2. List of Typhoon cases during observation.

Table 3. Detection counts and proportions for each flag from Oct 2003 to Dec 2022 (excluding NaN values).

Table 4: The differences in flag detection methods between TALOD and IOC.

https://doi.org/10.5194/egusphere-2024-3380
Preprint. Discussion started: 13 November 2024

List of Figures

Figure 1. The structure of I-ORS and Instruments (Right) and the horizontal distribution for bathymetry and the tracks of typhoon passed by I-ORS (data from Joint Typhoon Warning Center; cases depicted in Fig. 10). The star marks indicate the location of the I-ROS (red) and the Socheongcho (black; above) and Gageocho (black; below) Ocean Research Station, respectively. The black dots depict the locations of tide stations. The grey solid lines show the storm tracks passing by I-ROS from 2003 to 2022. The darker lines indicate the typhoon case in Table 2.

Figure 2. The circle markers indicate each process of methodological adjustment for the data before TP. The grey line with circles means the raw data and blue and red marker lines indicate the reverse and shift (+ 1.57m after reversed) process.

Figure 3. Flow chart of TALOD QC process.

Figure 4. Lines indicate the processes for fitting TPXO9 to observation (black line with circle) in the range check. (1) The blue line with a triangle means raw TPXO9 data. (2) The orange line with the square shows mean-shifted TPXO9 based on the Mean Square Error method. (3) The green line with a circle indicates the final output with a twice-smoothened bias added.

Figure 5. Time series for the examples of 4 flags. a) metadata, b) range, c) spike, and d) stuck. Each marker indicates Good Data (grey circle), metadata (blue circle), range (green triangle), spike (yellow square with red outline), and stuck (red cross), respectively.

Figure 6. Same as Fig. 5, but for Typhoon cases.

Figure 7. Representative results from 01 Apr 2012 to 15 Apr 2012

Figure 8. Same as Fig. 5, but for invariant stuck case (a-b, from 05 May 2005 to 07 May 2005), stuck case during short-period (c-d, from 12 Jul 2013 to 18 Jul 2013), range-spike misclassification case (e-f, from 12 Jun 2016 to 14 Jun 2016), and range-spike mixed case (g-h, 08 Sep 2016 to 13 Sep 2016). The figures on the left and right sides show results for TALOD and IOC, respectively.

Figure 9. Histogram of observed sea level anomaly without QC (light red) and with QC (light grey) from 2003 to 2022 at I-ORS. the area enclosed by a darker grey line indicates the normal distribution.

Figure 10. Time series of monthly QC-ed observations (black dot), Satellite (green empty circle), HYCOM (light red diamond), and GlORYS12 (light cyan hexagram) data during the observation period at the I-ORS.

Figure 11. Bar plot with error bar (A; Left) and Modified Taylor diagram (B; Right). the azimuthal angle represents the correlation coefficient, the radial distance indicates the standard deviation, and the

https://doi.org/10.5194/egusphere-2024-3380
Preprint. Discussion started: 13 November 2024

semicircles centered at the "OBS" marker mean the Root Mean Square Errors. The colors and markers indicate each data (black circle: observation, green square: Satellite, light cyan hexagram: GLORYS, purple pentagram: ORAS5, red diamond: HYCOM, light red upward-pointing triangle: HYCOM-R, light red downward-pointing triangle: HYCOM-S).

Figure 12. Monthly time series of sea level anomalies (left) and bar chart with error bar for sea level rise rate (right; units: mm/yr). Each color and type of line indicates the dataset (OBS: black solid line, Satellite: green solid line, Sum: bright red solid line, STERO: orange diamond, BARY: purple dotted line, GIA: sky-blue dotted line, and GNSS: bright brown).